Publishing Excellence Inspiring Progress
ARISTON PUBLICATIONS
MatSci Express
ISSN: 2997-8440 www.aristonpubs.com/matsci-express https://doi.org/10.69626/mse.2026.0105

RESEARCH ARTICLE

Effect of Dimensionality and Defect Engineering on Optical Absorption in MgS Nanostructures: A DFT and TD-DFT Study

Fotios I. Michos[1]*, Christina Papaspiropoulou[1], Nikos Aravantinos-Zafiris[2], Michail M. Sigalas[1]*

ABSTRACT: A systematic density functional theory and time-dependent density functional theory study of the optical absorption properties of MgS nanostructures with varying dimensionality and substitutional defect configurations is presented. Using the stoichiometric Mg_4S_4 nanoparticle as the fundamental building block, one-dimensional and two-dimensional MgS nanostructures were constructed through controlled geometric extension. Substitutional defects were also introduced by replacing Mg or S atoms with selected elements of the periodic table, enabling a comprehensive assessment of the effects of the size, the dimensions, the defect type, and the defect position. The results reveal that the extension to one-dimensional and two-dimensional geometries induces a pronounced red-shift of the absorption onset, accompanied by a substantial reduction of the HOMO–LUMO gap. These effects are further amplified by defect engineering, with proper element substitutions and positions of the defects, exhibiting particularly strong influence on low-energy absorption features. Overall, this study establishes clear structure related properties and demonstrates that the nanostructure dimensions in combination with the position of the defect could provide an effective strategy for tuning the optical absorption of MgS nanostructures toward lower energies.

Keywords: MgS nanostructures; Density functional theory; Time-dependent DFT; Optical absorption; Defect engineering; Dimensionality effects

Received: 12 February 2026; Revised: 01 April 2026; Accepted: 17 April 2026; Published Online: 08 May 2026

1. INTRODUCTION

Low-dimensional nanostructured materials have attracted significant attention over the past decades due to their unique electronic and optical properties, which often differ markedly from those of their bulk counterparts. Finite clusters, one-dimensional (1D) and two-dimensional (2D) nanostructures provide versatile platforms for tailoring electronic excitations through size, geometry, and chemical composition, making them promising candidates for optoelectronic and photonic applications, including light-emitting devices and solar energy conversion [1-3]. Among compound semiconductors, magnesium-based materials have been explored for their wide band gaps, chemical stability, and relevance in optoelectronic and energy-related technologies [4]. Magnesium oxide (MgO) nanoparticles (NPs) have gained significant attention through green synthesis methods for photocatalytic and biomedical applications [5 ,6]. Magnesium sulfide (MgS) nanoparticles, however, remain underexplored despite recent computational studies on their structural, optical, and vibrational properties [7], confirming the stability of Mg_4S_4-based low-dimensional architectures examined in this work. In addition, MgS has been investigated experimentally in thin films [8, 9], hierarchical nanostructures [10], and recently in MgS battery cathodes [11], demonstrating potential in optical devices,

[1] Department of Materials Science, University of Patras, Patras 26504, Greece.
[2] Department of Environment, Ionian University, Zakynthos, 29100, Greece.

* Author to whom correspondence should be addressed:
fotismixos@gmail.com (Fotios I. Michos)
sigalas@upatras.gr (Michail M. Sigalas)

© Ariston Publications 2026. All rights reserved.

phosphors, and energy storage [12].

At the nanoscale, MgS systems exhibit pronounced quantum confinement effects, which strongly influence their optical absorption characteristics [13]. A common strategy for understanding and tuning the optical properties of such systems is to start with small, well-defined stoichiometric clusters and systematically extend them toward lower-dimensional architectures [14]. Small clusters serve as fundamental building blocks, allowing for a clear interpretation of structure related properties before progressing to more complex geometries [7]. In this context, stoichiometric M_4X_4 clusters (where M is a metal and X a non-metal) have been widely used as reference systems for exploring size effects, dimensional growth, and defect-induced modifications [15 ,16]. Beyond size and dimensionality, defect engineering has emerged as a powerful approach for tuning the electronic and optical response of nanomaterials. Substitutional defects can introduce localized electronic states within the band gap, leading to reduced excitation energies and enhanced absorption in the visible region [17 ,18]. Such substitutions have been shown to play distinct roles, depending on the nature of the host lattice and the chemical characteristics of the dopant [19 ,20].

From a theoretical perspective, time-dependent density functional theory (TD-DFT) has become a standard tool for investigating the optical absorption properties of molecular clusters and nanostructures [21 ,22]. When combined with range-separated hybrid functionals, TD-DFT provides a reliable description of excitation energies, particularly for systems where long-range electron-hole interactions and charge-transfer effects are important [23 ,24]. This approach has been successfully applied to a wide range of low-dimensional materials, enabling detailed insights into the role of geometry and defects on optical spectra [25 ,26]. In recent studies, similar methodological frameworks have been employed to demonstrate how geometric dimensionality and substitutional defects can effectively shift the optical absorption of wide-gap nanoclusters toward lower energies [27 ,28]. These findings, combined with the experimental progress in related MgO systems [29], motivate the exploration of MgS nanostructures where analogous design principles may be applied computationally.

In this work, the focus is on Mg_xS_x nanostructures constructed from the stoichiometric Mg_4S_4 NP, which is adopted as a fundamental reference unit. Starting from this compact NP, one-dimensional and two-dimensional geometries are systematically generated, allowing for a controlled investigation of dimensionality effects on the optical absorption spectrum. In addition, substitutional defects were introduced at both Mg and S sites using a range of foreign atoms, enabling a comparative assessment of cationic and anionic defect engineering. The primary objective of this study is to demonstrate that the combined effects of geometry, dimensional extension, and substitutional defects can effectively drive the optical absorption of MgS nanostructures toward lower energies, approaching the visible region. By employing a consistent first-principles framework based on density functional theory (DFT) for ground-state properties and TD-DFT for excited-state calculations, a systematic and coherent study of how structural and chemical modifications influence the absorbance spectra of Mg_xS_x systems was developed.

2. COMPUTATIONAL METHODS

2.1. Ground-State Geometry Optimization

All ground-state calculations were performed within the framework of DFT. Geometry optimizations of all Mg_xS_x nanostructures were carried out using the generalized gradient approximation (GGA) with the Perdew–Burke–Ernzerhof (PBE) exchange–correlation functional [30]. The PBE functional was selected due to its well-documented reliability in describing the structural properties of ionic and semiconductor systems at moderate computational cost. All structures were treated as electrically neutral, and no symmetry constraints were imposed during the optimization process, allowing the systems to relax freely toward their minimum-energy configurations. A closed-shell formalism was employed throughout, as the primary focus of this work was the investigation of relative optical trends induced by geometry and substitution rather than magnetic effects.

Geometry optimizations were performed using the TURBOMOLE program package [31], which has been extensively used for first-principles calculations on molecular clusters and low-dimensional nanostructures [32 ,33]. The same atom-centered Gaussian basis set [34] was employed for all elements and all structures considered in this study, ensuring internal consistency across pristine, low-dimensional, and defect-containing systems [7]. Convergence criteria for total energies and atomic forces were chosen in accordance with standard TURBOMOLE defaults for reliable structural relaxation.

2.2. Optical Properties

Optical absorption properties of the optimized nanostructures were investigated using TD-DFT. All excited-state calculations were carried out with the Gaussian program package (Gaussian 16), by employing the range-separated hybrid CAM-B3LYP exchange–correlation functional [35]. The CAM-B3LYP functional has been shown to provide an improved description of excitation energies, particularly for systems where charge-transfer character and long-range electron–hole interactions play an important role [36 ,37]. For each structure, a sufficient number of low-lying singlet excited states was computed to construct the ultraviolet–visible (UV–Vis) absorption spectrum. The calculated vertical excitation energies and oscillator strengths were used to generate continuous absorbance spectra by applying Gaussian broadening to each electronic transition. This procedure enables a direct and physically meaningful comparison between different geometries and defect

 © Ariston Publications 2026. All rights reserved.

configurations. It should be emphasized that the present study focuses exclusively on electronic excitations and optical absorbance properties. Vibrational spectra, phonon modes, and infrared (IR) intensities were not considered, in contrast to studies addressing lattice dynamics or vibrational characteristics.

The investigated nanostructures were constructed using the Mg_4S_4 NP as an initial building block. Starting from this reference nanostructure, a series of 1D and 2D nanostructures were generated through systematic geometric extension. In addition, substitutional defects were introduced by replacing a single Mg or S atom with selected atoms from other elements, including Al, Na, Sc, Ti, Mn, Ag, F, and Cl, to examine the influence of both cases of substitutions on the optical response. In total, more than twenty distinct nanostructures were examined, encompassing pristine, low-dimensional geometries, and defect-containing configurations. All structural models were optimized and analyzed within the same computational framework, allowing for a consistent assessment of geometry-induced and defect-induced trends in the optical absorption spectra.

3. RESULTS AND DISCUSSION

3.1. Substitutional Defects in the Mg_4S_4 Reference NP

3.1.1. Substitution at S sites in Mg_4S_4

The effect of S-substitution on the optical properties of Mg_4S_4 was investigated first by replacing a single sulfur atom with N, F, or Cl. The optimized geometry of the reference NP Mg_4S_4 is presented in Figure 1(a) and a representative geometry of this group of NPs which was created by S-substitution is presented in Figure 1(b). The calculated absorbance spectra, together with that of the pristine Mg_4S_4 NP are shown in Figure 2. As illustrated in Figure 2, S-substitution leads to notable changes in the absorbance spectra, primarily through the appearance of additional absorption peaks across the examined energy range. For Mg_4S_3F and Mg_4S_3Cl, shown in Figures 2(b) and 2(c) respectively, distinct absorption peaks appear at energies around 0.8–0.9 eV, marking the onset of optical activity in these defected clusters. These low-energy features are not present in the pristine Mg_4S_4 structure, which shows negligible absorbance below 3.8 eV. Among the two halogen substitutions, Mg_4S_3Cl exhibits slightly stronger absorption intensity in the low-energy region, suggesting a more effective perturbation of the electronic structure. For the case of Mg_4S_3N, shown in Figure 2(d), the absorption onset is shifted only marginally toward lower energies, with the first notable features appearing above 3.2 eV. The dominant absorption peaks for this nanostructure are located at higher energies, primarily in the visible and near-UV region between 3.5 and 4.5 eV, indicating a comparatively smaller impact on gap narrowing.

Across all S-substituted structures, the resonances in the absorbance spectrum increased for higher energies, with multiple peaks observed between 2.5 and 5.0 eV. This behavior reflects the redistribution of oscillator strength and the formation of localized defect states associated with substitution at the S site. The corresponding HOMO–LUMO gaps, listed in Table 1, support these trends, showing that the S-substitution results in a smaller reduction of the gap compared to substitution at Mg sites. These results indicate that S-site substitution modifies the spectral shape and introduces new absorption features, although it is less effective in driving the absorption onset toward lower energies than Mg-site substitution as will be explained in the next paragraph.

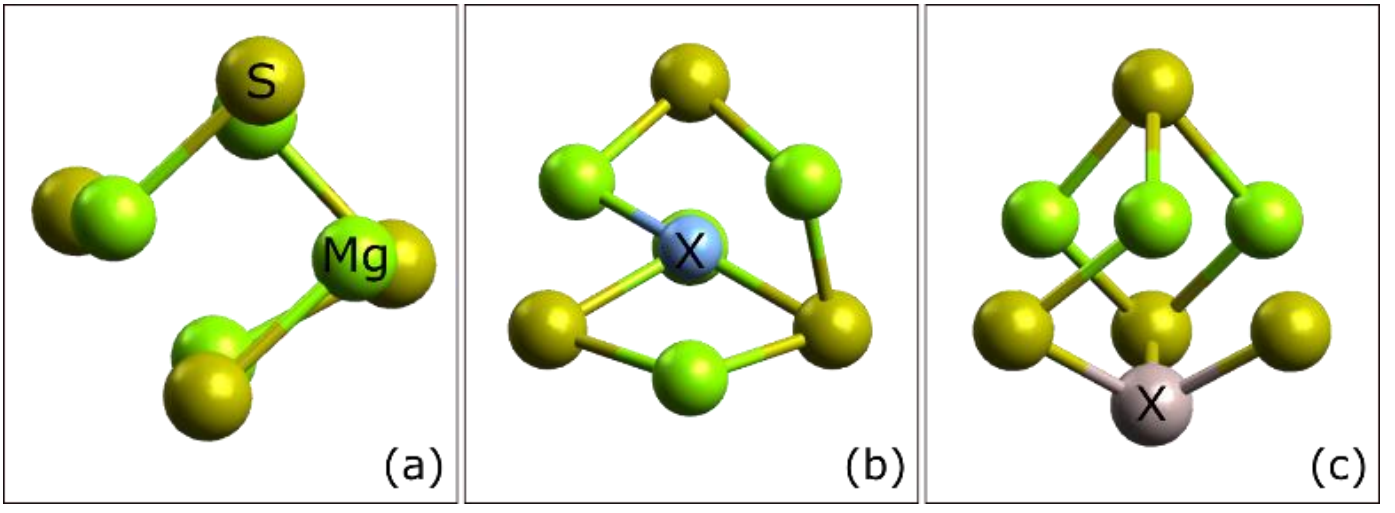

Fig. 1. (a) Top view of the optimized geometry of the Mg_4S_4 nanostructure which was used as the fundamental building block for the construction of the investigated nanostructures. (b) The defected structure of the general form Mg_4S_3X where an S atom was replaced by another atom X. For the examined cases X stands for Cl. F, N, and Ti. (c) Side perspective of the defected nanostructure of the general form Mg_3S_4X where a Mg atom was replaced by another atom X. For the examined cases X stands for Al, P, and Sc.

© Ariston Publications 2026. All rights reserved.

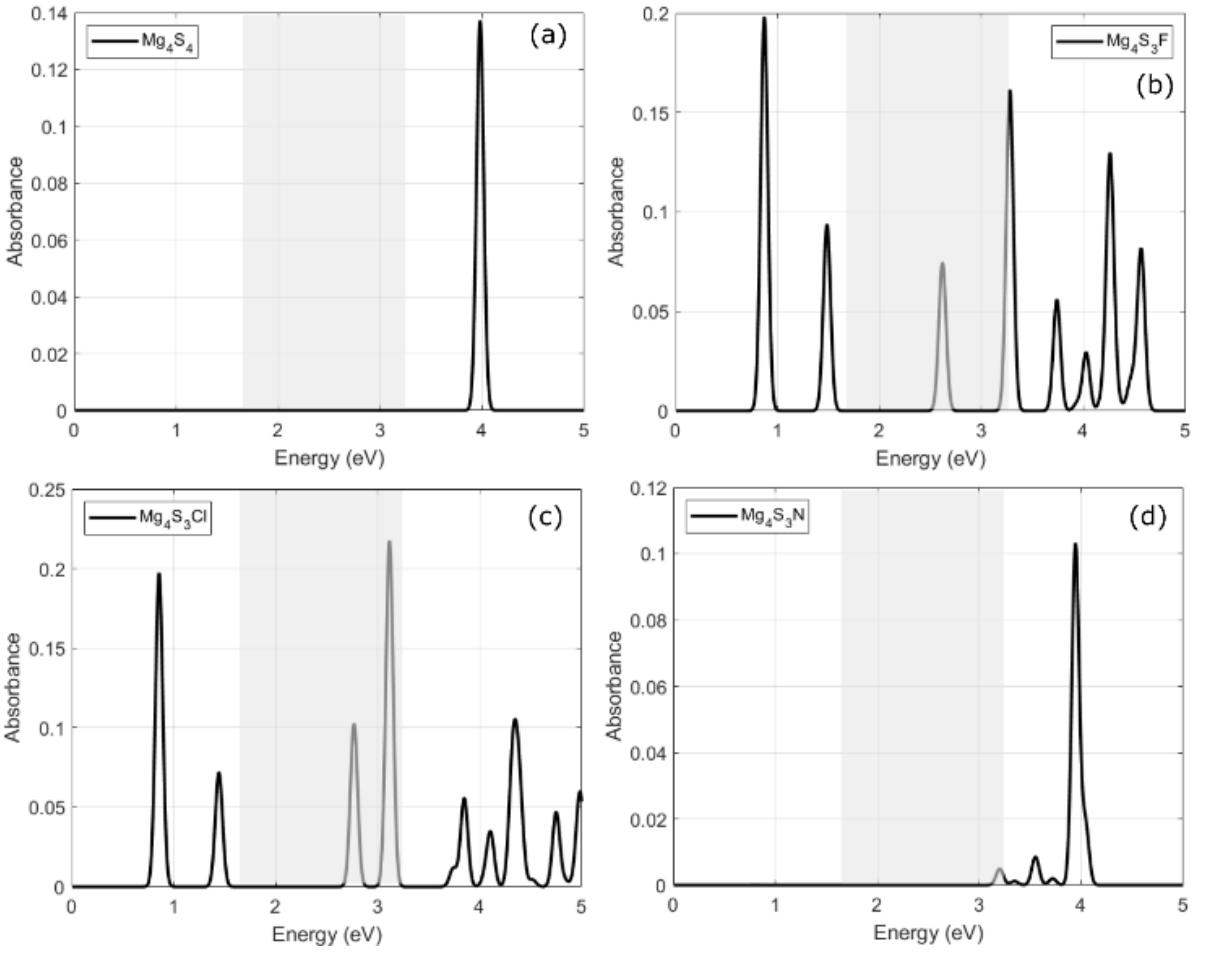

Fig. 2. The optical absorbance spectra for pristine Mg_4S_4 (a), and for nanostructures of the general form Mg_4S_3X where X stands for F (b), Cl (c), and N (d). The frequency zone in the grey background indicates the visible spectrum.

3.1.2. Substitution at Mg sites in Mg_4S_4

The study of the effect of substitutional defects on the optical absorption properties of the Mg_4S_4 reference NP was continued by replacing a single Mg atom with P, Sc, and Al. A representative optimized geometry of this group of NPs is shown in Figure 1(c), while the corresponding optical absorbance spectra are presented in Figure 3. As shown in Figure 3, all Mg-substituted Mg_4S_4 nanostructures exhibit a substantial modification of their absorbance spectrum compared to the pristine cluster. In particular, the absorption onset is significantly shifted toward lower energies, with the appearance of distinct low-energy absorption features below approximately 1.0 eV, which are absent in the undoped Mg_4S_4. Among the examined substitutions, the Ti-doped and Sc-doped NPs, presented in Figures 3(a) and 3(b) respectively, display the most pronounced red shift. For Mg_3S_4Ti NP, the first notable absorption peak appears at 0.48 eV, followed by additional features at 0.7 eV. Similarly, Mg_3S_4Sc exhibits low-energy absorption starting near 0.65 eV indicating a strong narrowing of the optical gap induced by these substitutions. These low-energy transitions should be attributed to defect-related electronic states introduced by the substituted atoms. The Mg_3S_4P structure, shown in Figure 3(c), also shows the emergence of new absorption peaks at low energies, with the absorption onset located at 1.42 eV, although the spectral intensity in this region is comparatively weaker than that observed for Sc substitution. In contrast, Al substitution leads to a more moderate red shift, with the first absorption features appearing at energies close to 1.85 eV, as presented in Figure 3(d), while still significantly lower than the pristine reference Mg_4S_4 NP.

For higher energies, all Mg-substituted NPs display a dense set of absorption peaks extending throughout the visible and near-ultraviolet region (approximately 1.5–4.5 eV), reflecting the increased density of electronic states and the lifting of degeneracies due to symmetry breaking. The redistribution of oscillator strength across the spectrum further highlights the strong impact of such substitutions on the electronic structure. The red shifts observed in the absorption onset correlate well with the reduction of the HOMO–LUMO gap reported in Table 1. In particular, Ti and Sc substitutions result in the largest gap narrowing, consistent with their enhanced low-energy optical activity. These results demonstrate that substitution at Mg sites is highly effective in tuning the optical response of the compact Mg_4S_4 cluster toward lower energies.

© Ariston Publications 2026. All rights reserved.

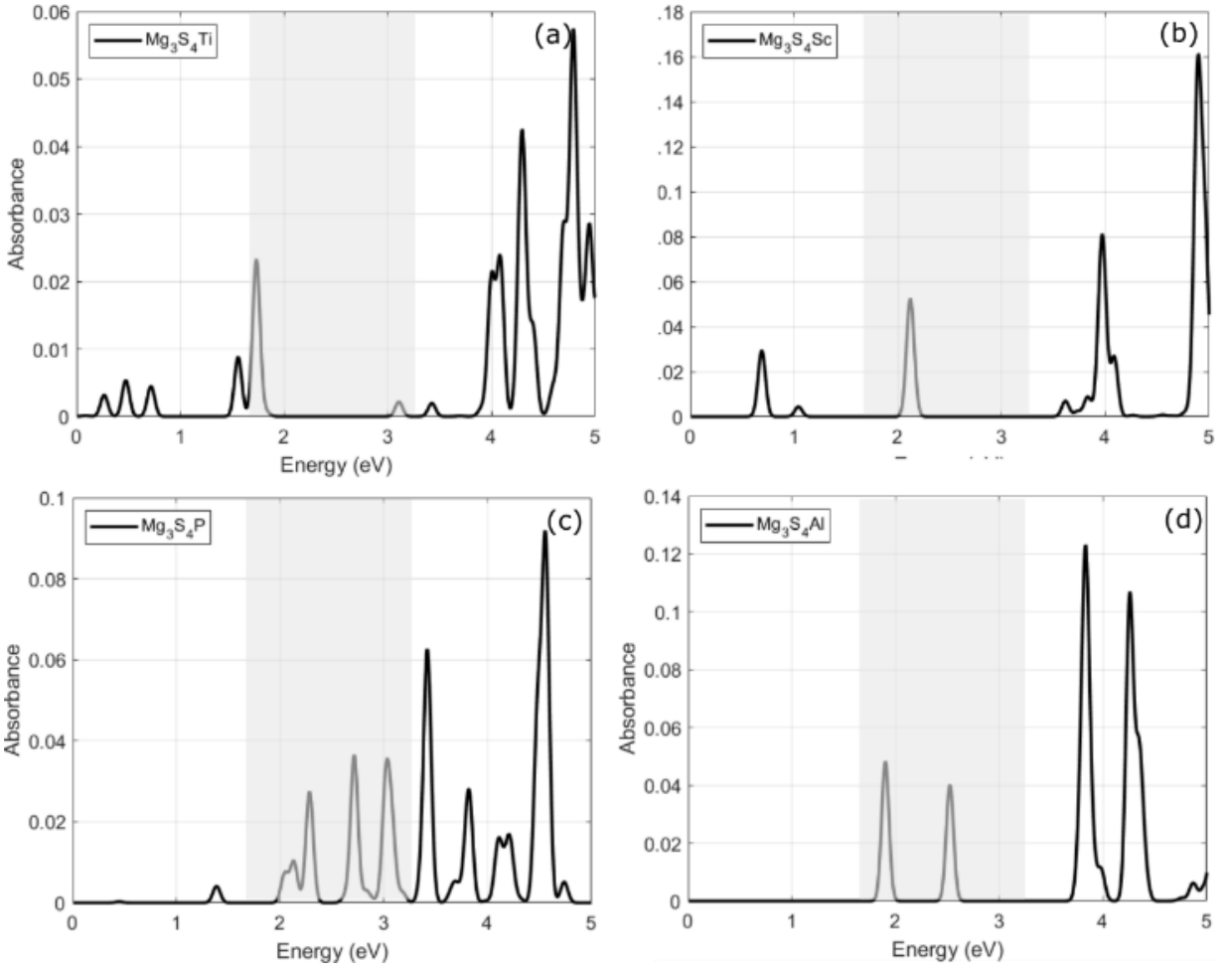

Fig. 3. The optical absorbance spectra for nanostructures of the general form Mg_3S_4X where X stands for Ti (a), Sc (b), P (c), and Al (d). The frequency zone in the grey background indicates the visible spectrum.

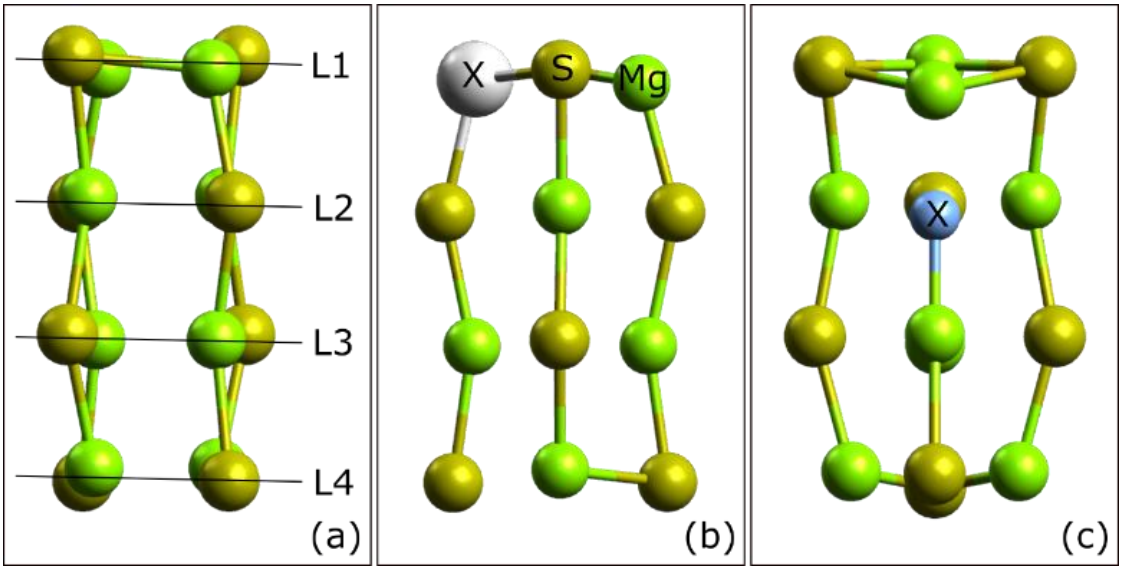

Fig. 4. (a) The optimized geometry of Mg_8S_8 nanostructure. The four layers (L) of the nanostructure where the substitution of a Mg or a S atom could be applied are also shown and labeled as Li, i=1-4. (b) Illustrating example of the defected nanostructure where the replacement was on layer L1. For this presented case, a Mg atom was replaced by another atom X, where X stands for Al and Sc. (c) Illustrating example of the defected nanostructure where the replacement was on layer L2. For the presented case a S atom was replaced by another atom X, where X stands for P, N, F, and Cl.

© Ariston Publications 2026. All rights reserved.

Table 1. Calculated HOMO-LUMO gaps (eV) for the pristine Mg_4S_4 reference cluster and substitutional defects at Mg and S sites (PBE level).

NP	HOMO – LUMO Gap (eV)
MgS	0.489
Mg_4S_4	2.956
Mg_3S_4Al	0.818
Mg_3S_4P	0.315
Mg_3S_4Na	2.872
Mg_3S_4Sc	0.357
Mg_3S_4Ti	0.414
Mg_4S_3Cl	0.573
Mg_4S_3F	0.550
Mg_4S_3N	0.955

3.2. Substitutional Defects in One-Dimensional Mg_8S_8 Nanostructures

The next group of the examined defected NPs was based on the one-dimensional Mg_8S_8 which was used as the fundamental building block for the construction of the investigated nanostructures. The defected NPs were built by substitution of one atom of the nanostructure in one of its four layers (L) as shown in Figure 4(a). In more detail, the substitution of a Mg or a S atom led to cases of the general form Mg_7S_8X-Li and Mg_8S_7X-Li. For the Mg_7S_8X-Li cases, a Mg atom was replaced by another atom X, where X stands for Al and Sc on the layer Li, where i=1-4. For the relevant cases of Mg_8S_7X-Li a S atom was replaced by another atom X where X stands for P, N, F, and Cl on the layer Li, where i=1-4. Illustrating examples of the defected nanostructures for cases of the general form Mg_7S_8X-L1 and Mg_8S_7X-L2 are presented in Figures 4(b) and 4(c) respectively. It should be noted that, due to the symmetry of the Mg_8S_8 NP, a substitution of an atom on L1 would be equal to a substitution on L4, and, relevantly, a substitution of an atom on L2 would be equal to a substitution on L3. Therefore, only cases of substitutions on L1 and L2 were examined in this part of the investigation.

3.2.1. Substitutional Defects on the first layer of Mg_8S_8

The Mg_8S_8 NP was created by elongating the initial cubic unit Mg_4S_4, as can be seen from Figure 4(a), and the absorbance spectrum of this NP is shown in Figure 5(a). Compared to the compact Mg_4S_4 NP, the one-dimensional Mg_8S_8 geometry already exhibits a denser distribution of absorption peaks, reflecting the increased delocalization of electronic states along the extended direction. In more detail, the Mg_8S_8 nanostructure exhibits its first significant absorption features at relatively high energies, with the absorption onset located at 4.2 eV, indicating a wide optical gap despite the one-dimensional extension. Due to the introduction of defects at layers L1 and L2 of the nanostructure, substantial modifications of the absorbance spectra were observed, including the emergence of pronounced low and intermediate energy absorption peaks. For substitutional defects at L1, as will be analyzed, a pronounced modification of the optical response was observed, characterized by a substantial red shift of the absorption onset and enhanced spectral intensity at low energies.

The substitutions at Mg sites introduce a distinct modification of the absorbance spectra. For the Mg_7S_8Sc-L1 NP, low-energy absorption features emerge in 1.5 eV, accompanied by additional peaks between 2.0 and 3.0 eV, as can be seen by the black line of Figure 5(b). For the Mg_7S_8Al-L1 nanostructure the calculated absorbance spectrum is presented by the black line in Figure 5(c). The spectrum shows a comparatively higher absorption onset, appearing at 2.5 eV, while still exhibiting a clear red shift relative to non-defected one-dimensional nanostructures. These features indicate a strong perturbation of the electronic structure associated with the presence of transition-metal atoms, consistent with the introduction of localized d-derived states.

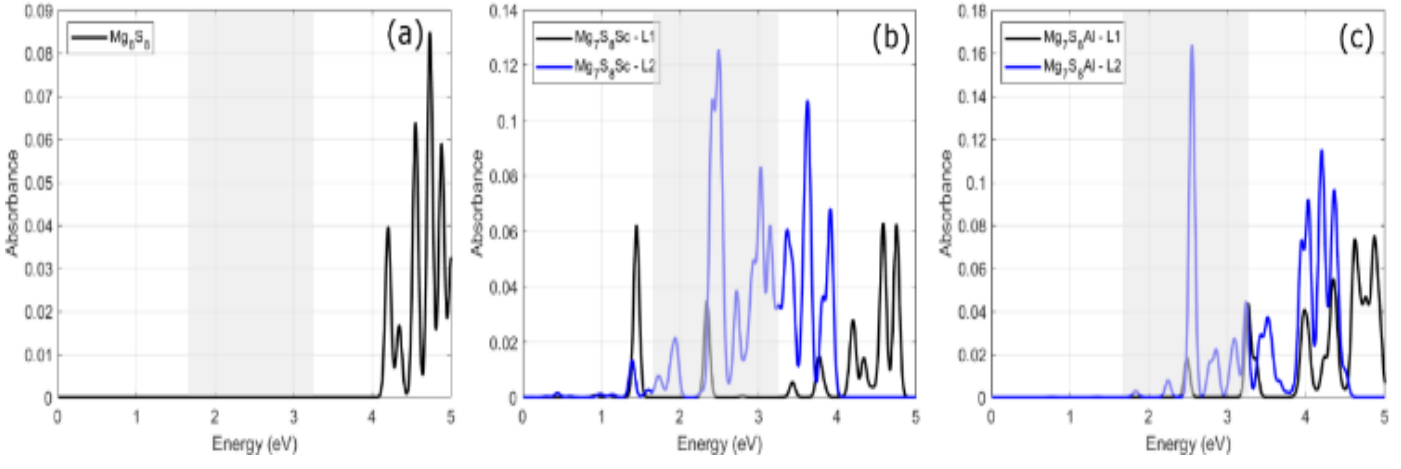

Fig. 5. The optical absorbance spectra for the pristine Mg_8S_8 (a), and for nanostructures of the general form Mg_7S_8X-Li where X stands for Sc (b) and Al (d). The frequency zone with grey background indicates the visible spectrum.

© Ariston Publications 2026. All rights reserved.

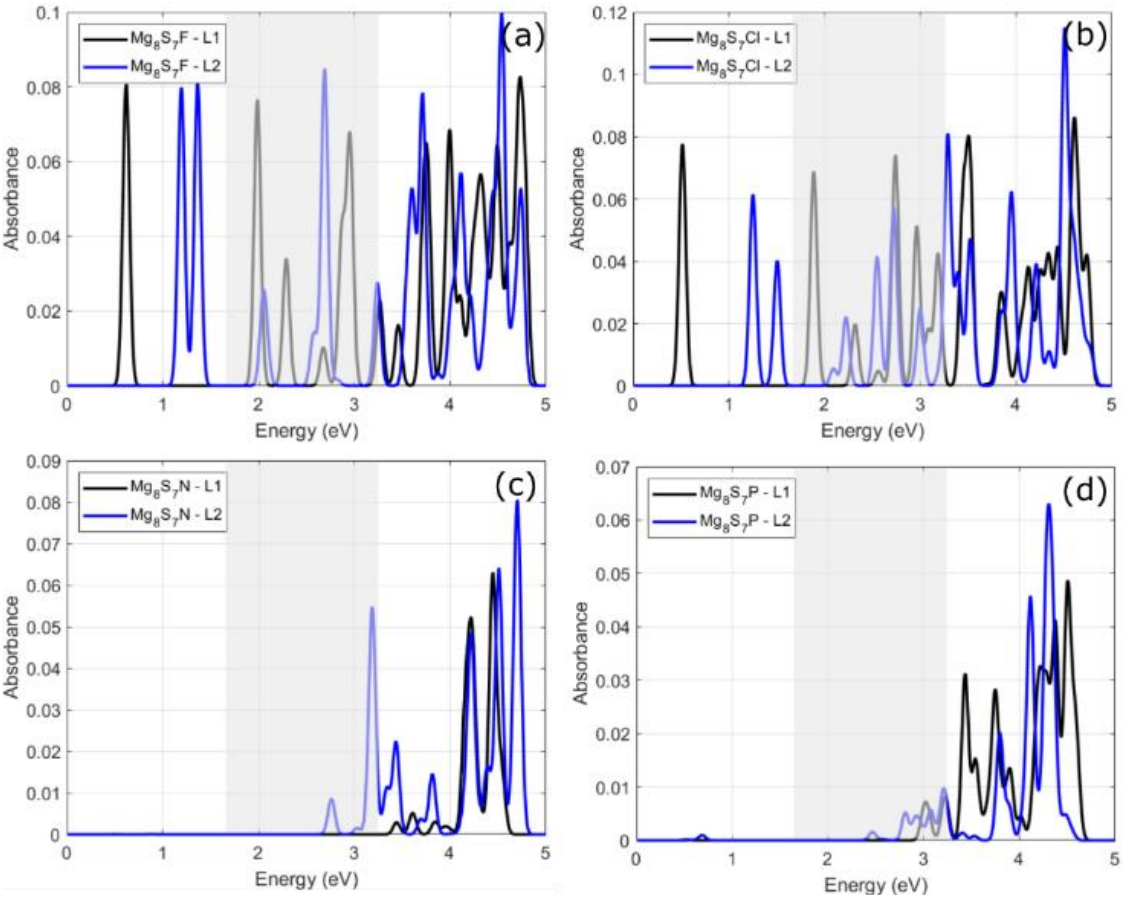

Fig. 6. The optical absorbance spectra for nanostructures of the general form Mg_8S_7X-Li where X stands for F (a), Cl (b), N (c), and P (d). The frequency zone with grey background indicates the visible spectrum.

The halogen substitutions at S sites of L1, named as Mg_8S_7F-L1 and Mg_8S_7Cl-L1 respectively, produce the most significant low-energy features, with distinct absorption peaks at 0.5–0.6 eV as shown in the black plots of Figures 6(a) and 6(b). These represent a more pronounced shift compared to pristine Mg_8S_8 and even outperform Mg_4S_4 defects, as described in Section 3.1 which were calculated between 0.4 and 0.9 eV, highlighting the synergistic effect of 1D extension and halogen defects. Secondary peaks at 1.8–2.2 eV indicate strong coupling of defect states to the extended backbone. Relevant substitutions with P and N also induce notable red shifts, although to a smaller extent. For the case of Mg_8S_7N-L1 NP, shown with the black plot of Figure 6(c), the first significant absorption peaks appear at slightly higher energies, around 3.4 eV, suggesting a more moderate narrowing of the optical gap compared to halogen substitution. For Mg_8S_7P-L1, presented by the black plot of Figure 6(d), the absorption onset is located at 2.9 eV, with multiple absorption features emerging throughout the visible region up to 4.6 eV.

At higher energies, all defect-containing Mg_8S_8 nanostructures display a dense set of absorption peaks extending from approximately 3.0 to 5.0 eV, reflecting the combined effects of reduced symmetry, dimensional extension, and defect-induced electronic states. The increased density of states in this energy range leads to a broadening of the optical response and enhanced absorbance across the visible and near-ultraviolet regions. The trends observed in the absorbance spectra are consistent with the corresponding HOMO–LUMO gaps reported in Table 2, which show a systematic reduction upon both dimensional extension and peripheral defect introduction. Notably, the combination of one-dimensional geometry and halogen substitution is particularly effective in driving the optical absorption of Mg_xS_x nanostructures toward low-energy and visible regimes.

Table 2. HOMO-LUMO gaps (eV) for pristine 1D Mg_8S_8 defected nanostructures where the substitutional defects at Mg/S sites are considered in L1 (PBE level).

NP	HOMO – LUMO Gap (eV)
Mg_8S_8	2.887
Mg_7S_8Sc	0.427
Mg_7S_8Al	0.813
Mg_8S_7F	0.431
Mg_8S_7Cl	0.414
Mg_8S_7P	0.779
Mg_8S_7N	0.745

© Ariston Publications 2026. All rights reserved.

3.2.2. Substitutional Defects on the second layer of Mg_8S_8

The study of the effect of defect positioning continued by introducing single substitutional defects at L2 of the Mg_8S_8 backbone. For this case, Mg atoms were replaced by Sc and Al, while S atoms were substituted by F, Cl, N, and P. The calculated absorbance spectra, compared to pristine Mg_8S_8 and the relevant L1 cases are presented in Figures 5 and 6 where the absorbance spectra of Mg_7S_8X-L2 and Mg_8S_7X-L2 cases are marked in blue.

Mg-substitutions in Mg_8S_8 result in a distinct and strong modification of the optical response. For Mg_7S_8Sc-L2 NP, shown by the blue plot of Figure 5(b), pronounced absorption peaks emerge as low as 1.35 eV, with additional intense features below 2.0 eV and throughout the 3.0–4.5 eV range. The Mg_7S_8Al-L2 NP exhibits a prominent peak at 2.5 eV with multiple higher-energy transitions as shown by the blue plot of Figure 5(c). Notably, substitution of a Mg atom by Sc at L2 produces significantly stronger low-energy intensity compared to both pristine Mg_8S_8 and corresponding L1 Sc defects, highlighting the critical role of defect proximity to the electronically active backbone.

Table 3. HOMO-LUMO gaps (eV) for pristine 1D Mg_8S_8 and relevant substitutional defects in L2 (PBE level).

NP	HOMO – LUMO Gap (eV)
Mg_7S_8Sc	0.198
Mg_7S_8Al	1.028
Mg_8S_7F	0.485
Mg_8S_7Cl	0.445
Mg_8S_7P	0.548
Mg_8S_7N	0.981
Mg_8S_8	2.887

Among the substitutions of S atoms at L2, Mg_8S_7F-L2 and Mg_8S_7Cl-L2 show a pronounced red shift of the absorption onset as presented in Figures 6(a) and 6(b). For Mg_8S_7F-L2, distinct absorption peaks appear at energies as low as 1.2–1.4 eV, followed by additional features at 2.1 eV. Similarly, Mg_8S_7Cl-L2 exhibits its first strong absorption peaks near 1.3–1.5 eV, indicating a substantial narrowing of the optical gap compared to the pristine nanostructure. These low-energy transitions are significantly more pronounced than those observed for the relevant P and N substitutions at L2. In more detail, for the cases of Mg_8S_7N-L2 and Mg_8S_7P-L2, presented by the blue plots of Figures 6(c) and 6(d) respectively, the absorption onset is shifted to intermediate energies, with the first notable peaks appearing at approximately 2.75 eV and 3.25 eV, respectively. Although these substitutions led to a denser absorbance spectrum compared to pristine Mg_8S_8, the red shift is less notable than that induced by halogen substitution, reflecting a more moderate perturbation of the electronic structure.

Overall, at higher energies, all L2 defected nanostructures display a dense distribution of absorption peaks between 3.0 and 5.0 eV, indicating increased electronic state density due to symmetry breaking and strong defect–host interactions. Thus, substitutional defects at the second layer of the nanoparticle induce more pronounced spectral restructuring than the relevant defects at the first layer, particularly in the intermediate energy range. The observed trends are consistent with the HOMO–LUMO gaps reported in Table 3, which show a further reduction for L2 defects relative to L1 substitutions. This behavior underscores the critical role of defect position in one-dimensional Mg_8S_8 nanostructures, demonstrating that interior layer defect engineering is a highly effective strategy for tuning optical absorption toward lower energies.

3.3. Defects in One-Dimensional $Mg_{16}S_{16}$

The study regarding the influence of nanostructure size on defect-induced optical tuning continued by using the one-dimensional extended $Mg_{16}S_{16}$ NP. The group of defected NPs of this part was extracted from the one-dimensional $Mg_{16}S_{16}$, named as $Mg_{16}S_{16}$-1D, by substitution of one atom of the nanostructure in one of its eight layers (L) as shown in Figure 7(a). According to the previous cases, the substitution of a Mg or a S atom led to cases of the general form $Mg_{15}S_{16}X$-Li and $Mg_{16}S_{15}X$-Li. It should be mentioned at this point that due to the size of the nanostructures, the relevant high computational cost and the available computational resources, there was a selection of the examined nanostructures. This selection was based on the results of the previous part of this study where the NPs were generated from the one-dimensional Mg_8S_8. Two of the most interesting cases of the previous part were Mg_8S_7F and Mg_8S_7Cl. The case where the substitution of the S atom is taking place on L1 is not expected to differ significantly from the cases which have already been examined, Mg_8S_7F-L1 and Mg_8S_7Cl-L1. As presented in Figures 6(a) and 6(b) and noted in the previous section, when the atom replacement is taking place on L2 there are also many resonances which appear within the visible spectrum. Thus, according to this numerical evidence, the selection of the examined cases was made by the replacement on layers L2 and L4. In more detail the examined cases of this part were $Mg_{16}S_{15}Cl$-L2 $Mg_{16}S_{15}Cl$-L4, and $Mg_{16}S_{15}F$-L4. The case of $Mg_{16}S_{15}Cl$-L2 would enable a straight comparison with the relevant case Mg_8S_7Cl-L2 of the previous examined group. The other two cases would provide numerical evidence regarding the substitution of a S atom on L4 which is the plane closest to the symmetry plane of the nanostructure. Illustrating examples of the defected nanoparticles for cases of the general form Mg_7S_8X-L2 and Mg_8S_7X-L4 are presented in Figures 7(b) and 7(c) respectively. It should be also noted that, due to the symmetry of the one-dimensional $Mg_{16}S_{16}$ NP, a substitution of an atom on L2 would be equal to a substitution on L7, and, relevantly, a substitution of an atom on L4 would be equal to a substitution on L5. Therefore, as already explained, only cases of substitutions on L2 and L4 were

© Ariston Publications 2026. All rights reserved.

examined in this part of the investigation.

The optical absorbance spectra of the examined NPs of this section are shown in Figure 8. The pristine one-dimensional $Mg_{16}S_{16}$-1D nanostructure, shown in Figure 8(a), exhibits its first significant absorption features at relatively high energies, with the absorption onset located at 4.2 eV, indicating that dimensional extension alone does not lead to substantial low-energy optical activity. The absorbance spectrum is dominated by sharp peaks in the high-energy region, characteristic of a wide-gap system with extended, still weakly perturbed electronic states. In contrast, the introduction of halogen substitutional defects leads to a pronounced modification of the optical response. Furthermore, halogen substitutions in extended $Mg_{16}S_{16}$-1D nanostructures maintain strong low-energy optical activity. The calculated absorbance spectra of all examined cases of this part which are $Mg_{16}S_{15}F$-L2, $Mg_{16}S_{15}Cl$-L2 and $Mg_{16}S_{15}Cl$-L4 are shown in Figures 8(b), 8(c), and 8(d) respectively. All cases exhibit prominent absorption peaks at 0.7-1.5 eV, with chlorine substitutions showing slightly higher intensity compared to fluorine at equivalent positions. These features represent a consistent extension of the low-energy response observed in Mg_8S_8 halogen defects, as presented in Section 3.2, demonstrating size-independent defect effectiveness across 1D Mg_xS_x architectures.

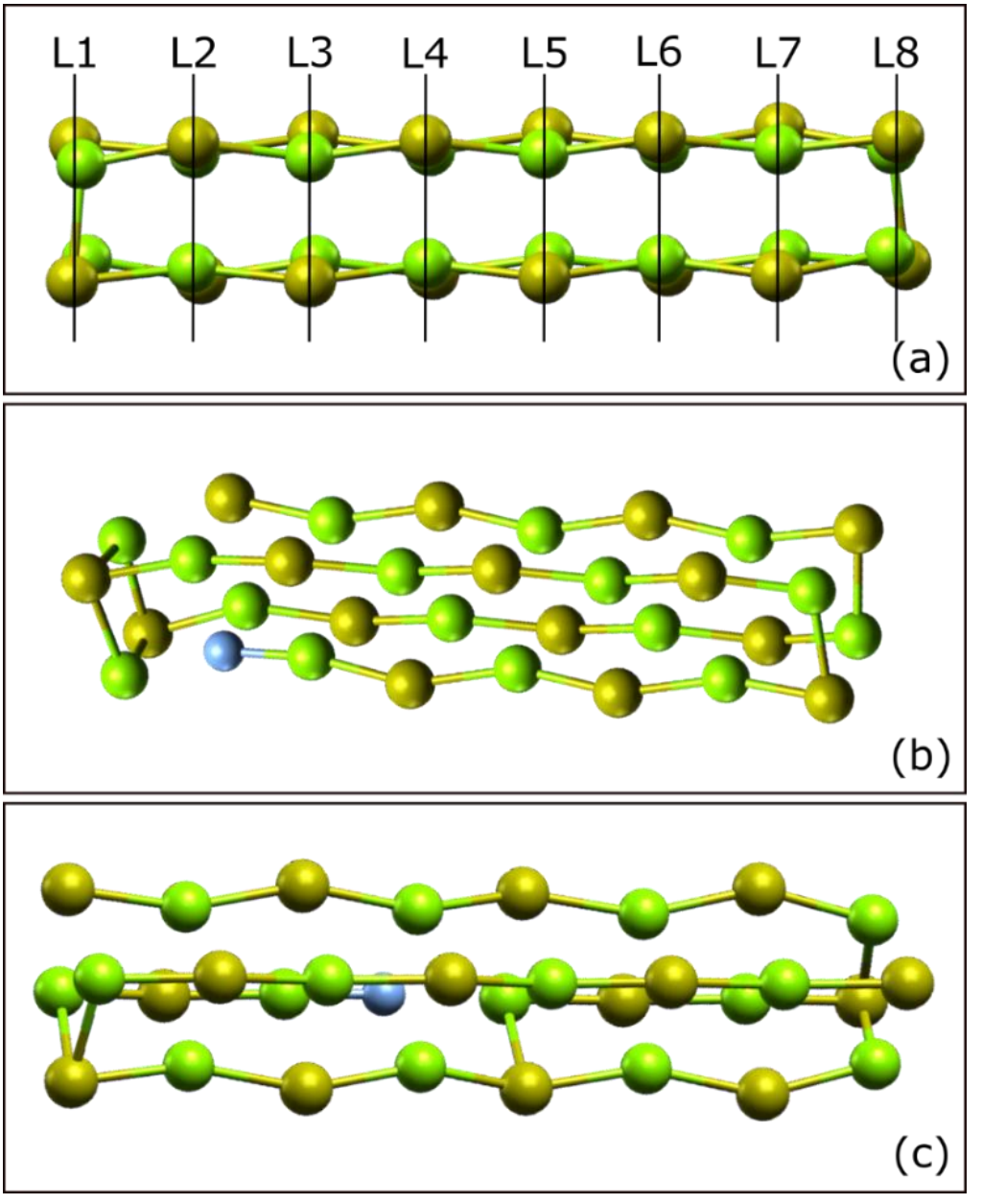

Fig. 7. (a) The optimized geometry of $Mg_{16}S_{16}$-1D nanostructure which was used as the fundamental building block for the construction of the nanostructures which were investigated in this part. The eight layers of the nanostructure where the substitution of a Mg or a S atom could be made are also shown and labeled as Li, i=1-8. Illustrating examples of the defected nanostructure where the replacement was on layer L2 (b) and L4 (c).

© Ariston Publications 2026. All rights reserved.

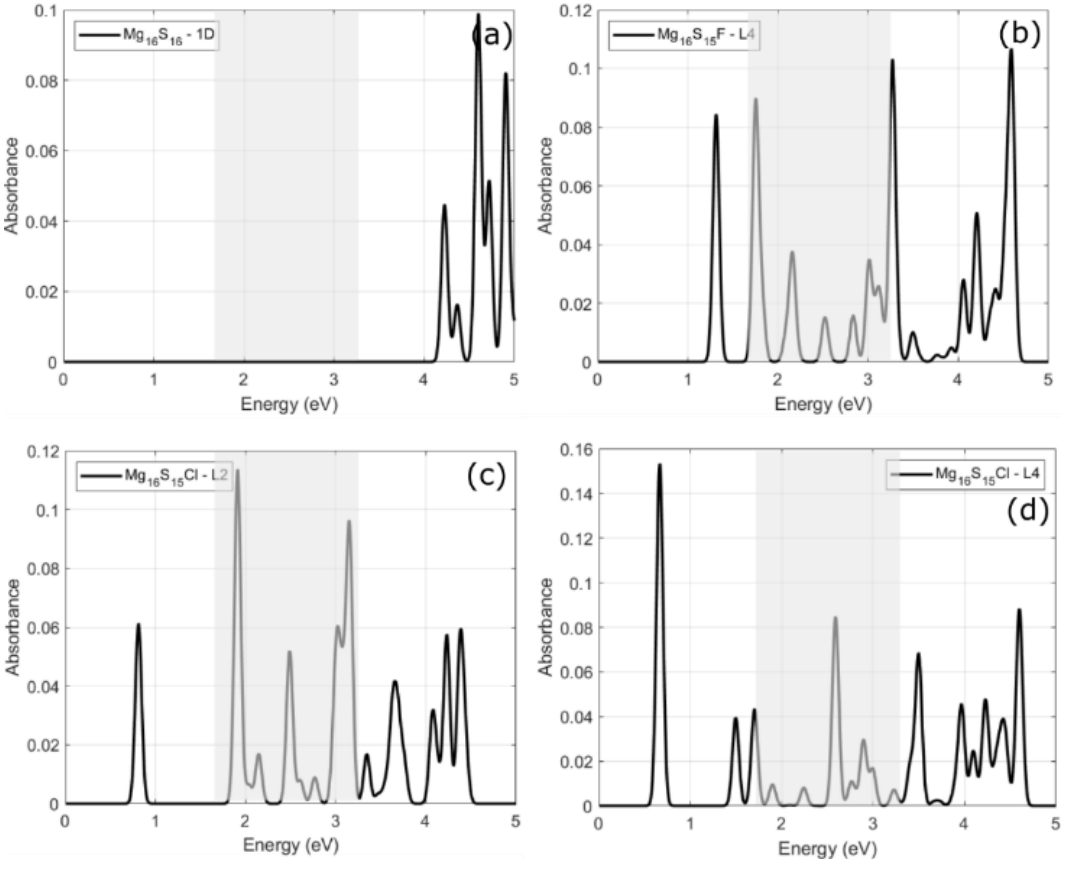

Fig. 8. The optical absorbance spectra for the pristine $Mg_{16}S_{16}$ – 1D (a), and for nanostructures of the general form $Mg_{16}S_{16}X$-Li where X stands for F (b) and Cl (c), (d). L2 and L4 indicate the layer of the structure in which the substitution of the atom was considered. The frequency zone with grey background indicates the visible spectrum.

Table 4. HOMO-LUMO gaps (eV) for pristine $Mg_{16}S_{16}$ and 1D nanostructures with F/Cl defects at different positions (PBE level).

NP	HOMO – LUMO Gap (eV)
Mg_8S_7F -L2	0.515
Mg_8S_7Cl -L2	0.462
Mg_8S_7Cl -L4	0.515
$Mg_{16}S_{16}$	2.914

The calculated absorbance spectra for both Cl-substituted nanostructures, $Mg_{16}S_{15}Cl$-L2 and $Mg_{16}S_{15}Cl$-L4, exhibit distinct low-energy absorption features that are absent in the pristine system. In more detail, $Mg_{16}S_{15}Cl$-L4 provides a strong absorption peak at 0.7 eV, representing a dramatic red shift of more than 3.5 eV relative to the pristine $Mg_{16}S_{16}$ structure. Additional absorption peaks appear in the 2.5–3.5 eV range, indicating the formation of defect-induced electronic states strongly coupled to the one-dimensional framework. The $Mg_{16}S_{15}Cl$-L2 structure also displays low-energy absorption, although with slightly reduced intensity and a somewhat higher onset energy, appearing at 0.8 eV. This difference highlights the strong dependence of the optical response on the defect position along the one-dimensional nanostructure, even when the same substituent atom is employed. The trends observed in the absorbance spectra are consistent with the HOMO–LUMO gaps reported in Table 4, which show a substantial reduction upon both size extension from Mg_8S_8 to $Mg_{16}S_{16}$ and the introduction of defects. Notably, the combination of one-dimensional extended geometry and defect position engineering proves to be highly effective in driving the optical absorption of MgS nanostructures deep into the low-energy and visible regimes.

3.4. Defects in Two-Dimensional $Mg_{16}S_{16}$

The final group of NPs which were examined was the two-dimensional case of $Mg_{16}S_{16}$, named as $Mg_{16}S_{16}$-2D. For this case, substitutions of a Mg or a S atom on the cubic unit of the structure, as shown in Figure 9(a), led to the defected cases of this group. In more detail, as shown in the inset of Figure 9(a), atom replacements were performed for Mg or S atoms in positions named as 1, 2, and 3 respectively in each case in the cubic unit of the nanostructure. Thus, the nanostructures $Mg_{15}S_{16}Al$-3 and $Mg_{15}S_{16}Sc$-3 were created by substitution of a Mg by an Al and a Sc atom on position 3. In the same frame $Mg_{16}S_{15}F$-2, $Mg_{16}S_{15}Cl$-2, and $Mg_{16}S_{15}Cl$-3 where the examined NPs which were extracted by

 © Ariston Publications 2026. All rights reserved.

substitution of a Sc atom by a F or a Cl atom on positions 2 and 3 respectively, as shown in the inset of Figure 9(a). According to the available computational resources the selected nanostructures were based upon the already examined cases of the previous groups that provided the most interesting results. Therefore, the selection of Sc and Al for replacement of a Mg atom and Cl and F for replacement of S atom. In addition, the replacement of a Mg or a S atom on positions 2 and 3, as shown in Figure 9, represents cases where the defected atom will have 4 or 5 bonds instead of three bonds of position 1. It should be also mentioned at this point that, due to the symmetry on the geometry of the structure, the performed replacements on the indicated cubic unit are equivalent to relevant replacements on the other three cubic units of the nanostructure.

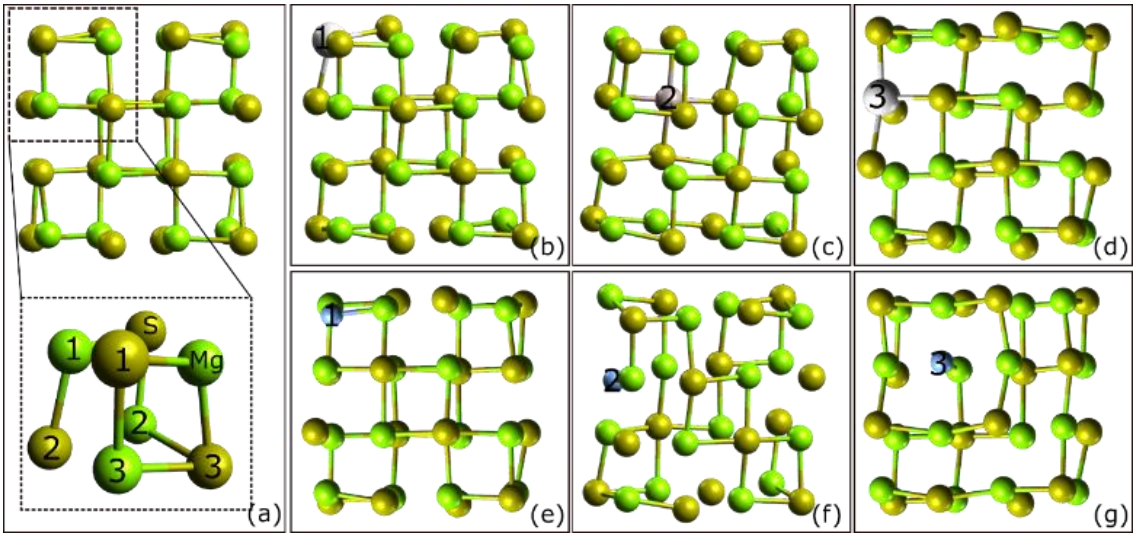

Fig. 9. (a) Optimized geometry of the two-dimensional $Mg_{16}S_{16}$-2D nanostructure in which substitutional defects at Mg and S sites were obtained by replacing a single Mg or S atom from the cubic unit which is marked with the dashed line. The substitution of the Mg (or S) atom was considered at positions 1, 2, and 3 of the cubic unit as shown in the inset. Cases for Mg substitution in position 1 (b), 2 (c), and 3 (d). Cases for S substitution in position 1 (e), 2 (f), and 3 (g).

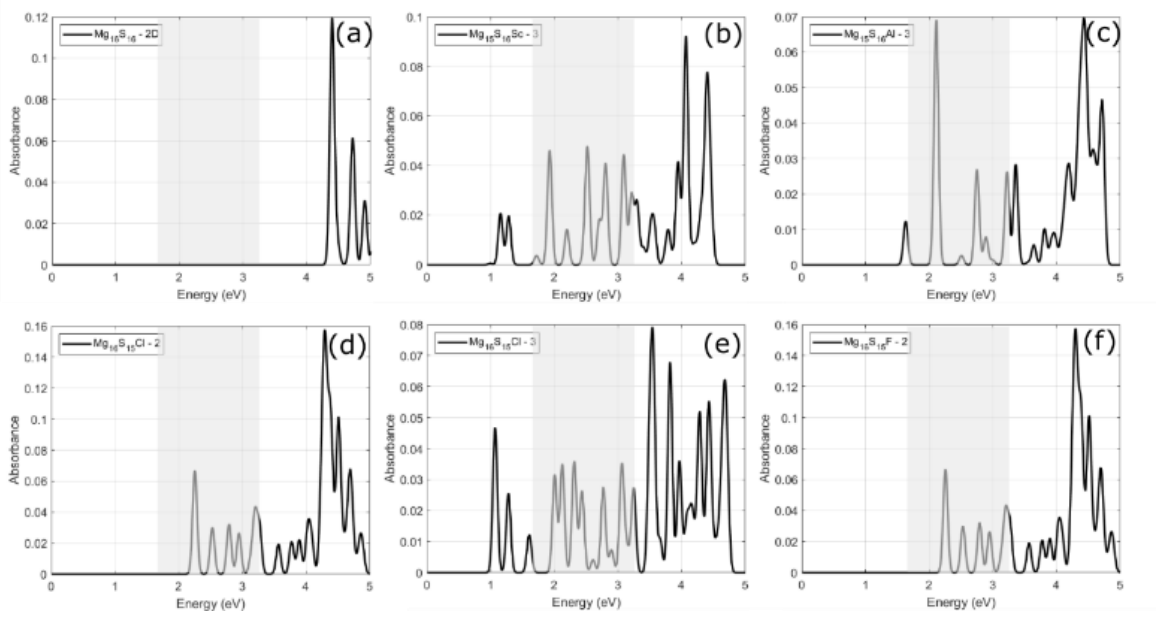

Fig. 10. Top: The calculated optical absorbance spectra for the two-dimensional $Mg_{16}S_{16}$-2D (a), and for nanostructures of the general form $Mg_{15}S_{16}X$-Y where X stands for Sc (b) and Al (c). Bottom: The calculated optical absorbance spectra for nanostructures of the general form $Mg_{16}S_{15}X$-Y where X stands for Cl (d), (e), and F (f). For all cases Y indicates the position of the cubic unit of the structure in which the substitution of the atom was considered named as 1, 2, and 3 as explained in Figure 9. The frequency zone with grey background indicates the visible spectrum.

© Ariston Publications 2026. All rights reserved.

The calculated optical absorbance spectra are shown in Figure 10, together with the case of the $Mg_{16}S_{16}$-2D nanostructure. The pristine $Mg_{16}S_{16}$-2D exhibits an absorption onset located at 4.4 eV, with intense peaks appearing predominantly in the high-energy region as shown in the plot of Figure 10(a). Compared to its one-dimensional counterpart, the 2D structure shows a slightly denser absorption profile at higher energies, reflecting enhanced electronic delocalization within the planar geometry while maintaining a relatively wide optical gap.

The introduction of defects led to a substantial modification of the optical response. Substitution of Mg with Sc and Al significantly alters the optical response as presented in the top row of Figure 10. The absorbance spectrum of $Mg_{15}S_{16}Sc$-3, shown in Figure 10(b), exhibits multiple absorption peaks throughout the visible region, with a prominent feature at 1,2 eV and additional transitions in the 2.0–3.0 eV range. Similarly, the absorbance of $Mg_{15}S_{16}Al$-3, shown in Figure 10(c), provides enhanced absorption across a broad energy window, with characteristic peaks at 1.6 eV and 2.1 eV, indicating effective hybridization between defect states and the host electronic structure.

Chlorine substitution has a pronounced effect, particularly for the $Mg_{16}S_{15}Cl$-2 nanostructure, shown in Figure 10(d), which displays a strong absorption peak near 4.3–4.4 eV with a maximum absorbance approaching 0.16, representing the most intense feature among all examined 2D systems. Additional absorption peaks emerge in the 2.0–3.0 eV range, indicating the presence of defect-induced electronic states within the pristine gap. It should be noted, however, that the first peak appears at 2.25 eV. The $Mg_{16}S_{15}Cl$-3 structure also shows enhanced optical activity compared to the pristine system, with distinct absorption features appearing at approximately 1.0–1.2 eV, followed by strong transitions near 3.5–3.8 eV, as shown in the plot of Figure 10(e). The lower-energy onset compared to the pristine structure suggests that defect position within the 2D lattice plays a critical role in determining the degree of band-gap reduction.

Overall, S-substitution in $Mg_{16}S_{16}$-2D NP results in a clear reduction of the effective optical gap and a significant increase in absorption intensity across the visible and near-UV regions. Compared to one-dimensional NPs, the 2D geometry promotes stronger electronic delocalization, leading to higher absorbance values and a denser distribution of optical transitions. These findings demonstrate that combined control of dimensionality and defect chemistry provides a powerful strategy for tailoring the optical properties of MgS nanostructures.

For the sake of completeness, the effect of atom substitutions on the electronic properties of $Mg_{16}S_{16}$-2D NP was further analyzed through the calculated HOMO–LUMO energy gaps, which are presented in Table 5. The pristine $Mg_{16}S_{16}$-2D structure exhibits a relatively large HOMO–LUMO gap of 2.927 eV, consistent with its wide-gap semiconducting character. Substitution at Mg sites leads to a pronounced reduction of the gap. In particular, Sc substitution results in very small HOMO–LUMO gap 0.453 eV, indicating the introduction of mid-gap states and enhanced electronic delocalization. Al substitution also significantly narrows the gap with value 0.649 eV reflecting a strong sensitivity of the electronic structure to both dopant type and position. In contrast, substitution at S sites induces more moderate gap reductions. The Mg_8S_7F structures exhibit HOMO–LUMO gaps of 0.653 eV, 0.665 eV, and 0.285 eV, while the corresponding Mg_8S_7Cl systems show gaps of 0.575 eV, 0.761 eV, and 0.299 eV. Overall, cationic substitution produces a stronger gap narrowing compared to anionic substitution, highlighting the dominant role of Mg-site defects in tuning the electronic properties of two-dimensional Mg–S nanostructures.

Table 5. HOMO-LUMO gaps (eV) for pristine 2D $Mg_{16}S_{16}$ and substitutional defects at Mg sites with F, Cl, Sc, Al (PBE level).

NP	HOMO – LUMO Gap (eV)
$Mg_{16}S_{15}F$ -2	0.653
$Mg_{16}S_{15}Cl$ -3	0.299
$Mg_{16}S_{15}Cl$ -2	0.575
$Mg_{15}S_{16}Sc$ -3	0.453
$Mg_{15}S_{16}Al$ -3	0.649
$Mg_{16}S_{16}$-2D	2.927

4. CONCLUSIONS

In this work, a systematic first-principles investigation of the optical absorption properties of MgS nanostructures with different dimensions and defect configurations was carried out using density functional theory and time-dependent DFT calculations. Starting from the cubic unit Mg_4S_4 as the fundamental building block, a series of one-dimensional and two-dimensional MgS nanostructures were constructed, enabling a controlled exploration of size, dimensionality, and defect-induced effects on their electronic and optical behavior. The results demonstrate that both dimensionality extension and substitutional defect engineering play a crucial role in tailoring the optical response of MgS systems. The transition from the initial unit Mg_4S_4 to extended one-dimensional and two-dimensional geometries leads to a pronounced red-shift of the absorption onset, accompanied by a substantial reduction of the HOMO–LUMO gap. These effects are further enhanced upon the introduction of substitutional defects, with defect positions exhibiting particularly strong influence on the emergence of low-energy absorption features.

Notably, one-dimensional $Mg_{16}S_{16}$ nanostructures with position-controlled halcogen defects and two-dimensional $Mg_{16}S_{16}$ systems with Mg-substitutions were both found to display optical absorption extending deep into the low-energy and near-visible regions. The observed trends are fully consistent with the calculated HOMO–LUMO gaps, highlighting the strong interplay between structural extension, defect position, and electronic structure

© Ariston Publications 2026. All rights reserved.

modulation.

Overall, this study establishes a clear structure related properties for MgS nanostructures and demonstrates that the combined control of dimensionality and substitutional defect positioning provides an effective strategy for tuning optical absorption toward lower energies. These findings underline the potential of defect-engineered MgS nanostructures for optoelectronic and photonic applications and provide a robust theoretical framework for the rational design of low-dimensional metal–chalcogenide materials with tailored optical properties.

DECLARATIONS

Ethical Approval

We affirm that this manuscript is an original work, has not been previously published, and is not currently under consideration for publication in any other journal or conference proceedings. All authors have reviewed and approved the manuscript, and the order of authorship has been mutually agreed upon.

Funding

This research received no external funding.

Availability of data and material

The data presented in this study are available on request from the corresponding author. The data are not publicly available due to the extremely large size.

Conflicts of Interest

The authors declare no conflicts of interest.

Author's contribution statement

Conceptualization, F.I.M., C.P., N.A-Z and M.M.S.; methodology, F.I.M., C.P., N.A-Z and M.M.S.; software, F.I.M., C.P., N.A-Z and M.M.S.; validation, F.I.M., C.P., N.A-Z and M.M.S.; formal analysis, F.I.M., C.P., N.A-Z and M.M.S.; investigation, F.I.M., C.P., N.A-Z and M.M.S.; resources, F.I.M., C.P., N.A-Z and M.M.S.; data curation, F.I.M., C.P., N.A-Z and M.M.S.; writing—original draft preparation, F.I.M., C.P., N.A-Z and M.M.S.; writing—review and editing, F.I.M., C.P., N.A-Z and M.M.S.; visualization, F.I.M., C.P., N.A-Z and M.M.S.; supervision, F.I.M., C.P., N.A-Z and M.M.S.; project administration, F.I.M., C.P., N.A-Z and M.M.S.; funding acquisition, F.I.M., C.P., N.A-Z and M.M.S. All authors have read and agreed to the published version of the manuscript.

Data availability statement

The data supporting the findings of this study are available from the corresponding author upon reasonable request.

REFERENCES

[1] Castleman, A.W. and Bowen, K., **1996**. Clusters: Structure, energetics, and dynamics of intermediate states of matter. *The Journal of Physical Chemistry*, *100*(31), pp.12911-12944. https://doi.org/10.1021/jp961030k

[2] Jena, P. and Sun, Q., **2018**. Super atomic clusters: design rules and potential for building blocks of materials. *Chemical reviews*, *118*(11), pp.5755-5870. https://doi.org/10.1021/acs.chemrev.7b00524

[3] Özgür, Ü., Alivov, Y.I., Liu, C., Teke, A., Reshchikov, M.A., Doğan, S., Avrutin, V.C.S.J., Cho, S.J. and Morkoç, A.H., **2005**. A comprehensive review of ZnO materials and devices. *Journal of applied physics*, *98*(4). https://doi.org/10.1063/1.1992666

[4] Pauly, S., Gorantla, S., Wang, G., Kühn, U. and Eckert, J., **2010**. Transformation-mediated ductility in CuZr-based bulk metallic glasses. *Nature materials*, *9*(6), pp.473-477. https://doi.org/10.1038/nmat2767

[5] Rashid, S., Islam, S., Qamer, S., Ali, M., Fatima, M., Javaid, L., Ali, A., Sarwar, A. and Farooq, A.S., **2025**. A review of green synthesized magnesium oxide nanoparticles coated textiles. *Journal of Industrial Textiles*, *55*, p.15280837251313518. https://doi.org/10.1177/15280837251313518

[6] Singaravelu, S., Motsoene, F., Abrahamse, H. and Dhilip Kumar, S.S., **2025**. Green-synthesized metal nanoparticles: a promising approach for accelerated wound healing. *Frontiers in bioengineering and biotechnology*, *13*, p.1637589. https://doi.org/10.3389/fbioe.2025.1637589

[7] Aravantinos-Zafiris, N., Michos, F.I. and Sigalas, M.M., **2024**. Vibrational Spectrum of Magnesium Monochalcogenide Nanoparticles. *Nanomaterials*, *14*(23), p.1918. https://doi.org/10.3390/nano14231918

[8] Aravantinos-Zafiris, N., Chronis, A.G. and Sigalas, M.M., **2021**. Structural and optical properties of exotic magnesium monochalcogenide nanoparticles. *Materials Today Communications*, *28*, p.102622. https://doi.org/10.1016/j.mtcomm.2021.102622

[9] Sood, S., Kumar, P., Raina, I., Misra, M., Kaushal, S., Gaur, J., Kumar, S. and Singh, G., **2025**, May. Enhancing optoelectronic performance through rare-earth-doped ZnO: insights and applications. In

© Ariston Publications 2026. All rights reserved.

Photonics (Vol. 12, No. 5, p. 454). MDPI. https://doi.org/10.3390/photonics12050454

[10] Chopra, S., Pande, K., Kumar, V.S. and Sharma, J.A. eds., **2022**. *Novel Applications of Carbon Based Nano-Materials*. CRC Press.

[11] Choudhary, S., Oli, N., Shweta, S., Kumar, S., Bhattarai, M.K., Malca-Reyes, C.A., Katiyar, R.K., Tripathi, B., Díaz-Vázquez, L.M., Morell, G. and S. Katiyar, R., **2024**. Encapsulation Engineering of Sulfur into Magnesium Oxide for High Energy Density Li–S Batteries. *Molecules*, *29*(21), p.5116. https://doi.org/10.3390/molecules29215116

[12] Salvatella, G., Gort, R., Bühlmann, K., Däster, S., Vaterlaus, A. and Acremann, Y., **2016**. Ultrafast demagnetization by hot electrons: Diffusion or super-diffusion?. *Structural Dynamics*, *3*(5). https://doi.org/10.1063/1.4964892

[13] Orek, C., Keser, S., Kaygili, O., Zuchowski, P. and Bulut, N., **2023**. Structures and optical properties of zinc oxide nanoclusters: a combined experimental and theoretical approach. *Journal of Molecular Modeling*, *29*(8), p.227. https://doi.org/10.1007/s00894-023-05641-1

[14] Xie, H., Li, Z., Cheng, L., Haidry, A.A., Tao, J., Xu, Y., Xu, K. and Ou, J.Z., **2022**. Recent advances in the fabrication of 2D metal oxides. *Iscience*, *25*(1). https://doi.org/10.1016/j.isci.2021.103598

[15] Bubanja, V., **2008**. Virtual electron diffusion through a quantum dot in the presence of electromagnetic fluctuations. *Physical Review B—Condensed Matter and Materials Physics*, *78*(15), p.155423. https://doi.org/10.1103/PhysRevB.78.155423

[16] Couliou, M. and Monchaux, R., **2015**. Large-scale flows in transitional plane Couette flow: a key ingredient of the spot growth mechanism. *Physics of Fluids*, *27*(3). https://doi.org/10.1063/1.4914082

[17] Galbiati, M., Ferrier, L., Solnyshkov, D.D., Tanese, D., Wertz, E., Amo, A., Abbarchi, M., Senellart, P., Sagnes, I., Lemaître, A. and Galopin, E., **2012**. Polariton condensation in photonic molecules. *Physical review letters*, *108*(12), p.126403. https://doi.org/10.1103/PhysRevLett.108.126403

[18] Van de Walle, C.G., **2000**. Hydrogen as a cause of doping in zinc oxide. *Physical review letters*, *85*(5), p.1012. https://doi.org/10.1103/PhysRevLett.85.1012

[19] Janotti, A. and Van de Walle, C.G., **2009**. Fundamentals of zinc oxide as a semiconductor. *Reports on progress in physics*, *72*(12), p.126501. https://doi.org/10.1088/0034-4885/72/12/126501

[20] Desnica, U.V., **1998**. Doping limits in II–VI compounds—Challenges, problems and solutions. *Progress in crystal growth and characterization of materials*, *36*(4), pp.291-357. https://doi.org/10.1016/S0960-8974(98)00011-4

[21] Chong, D.P., **1995**. Recent advances in density functional methods.

[22] Runge, E. and Gross, E.K., **1984**. Density-functional theory for time-dependent systems. *Physical review letters*, *52*(12), p.997. https://doi.org/10.1103/PhysRevLett.52.997

[23] Yanai, T., Tew, D.P. and Handy, N.C., **2004**. A new hybrid exchange–correlation functional using the Coulomb-attenuating method (CAM-B3LYP). *Chemical physics letters*, *393*(1-3), pp.51-57. https://doi.org/10.1016/j.cplett.2004.06.011

[24] Li, L., Meller, G. and Kosina, H., **2008**. Transport energy in organic semiconductors with partially filled localized states. *Applied Physics Letters*, *92*(1). https://doi.org/10.1063/1.2829863

[25] Dreuw, A. and Head-Gordon, M., **2005**. Single-reference ab initio methods for the calculation of excited states of large molecules. *Chemical reviews*, *105*(11), pp.4009-4037. https://doi.org/10.1021/cr0505627

[26] Wang, L., Wen, J., He, H. and Zhang, J., **2013**. A dual-level direct dynamics study on the hydrogen abstraction reaction of oxygen atom with methylhydrazine. *International Journal of Quantum Chemistry*, *113*(21), pp.2338-2344. https://doi.org/10.1002/qua.24458

[27] Brieler, F.J., Grundmann, P., Fröba, M., Chen, L., Klar, P.J., Heimbrodt, W., Krug von Nidda, H.A., Kurz, T. and Loidl, A., **2005**. Comparison of the magnetic and optical properties of Wide-Gap (II, MN) VI nanostructures confined in mesoporous silica. *European journal of inorganic chemistry*, *2005*(18), pp.3597-3611. https://doi.org/10.1002/ejic.200500366

[28] Zhang, C., Yoon, B. and Landman, U., **2007**. Predicted oxidation of CO catalyzed by Au nanoclusters on a thin defect-free MgO film supported on a Mo (100) surface. *Journal of the American Chemical Society*, *129*(8), pp.2228-2229. https://doi.org/10.1021/ja0684545

[29] Fan, Z., Li, R., Zhang, X., Zhao, W., Pan, Z. and Yang, X., **2025**. Defect engineering: can it mitigate strong coulomb effect of Mg2+ in cathode materials for rechargeable magnesium batteries?. *Nano-Micro Letters*, *17*(1), p.4. https://doi.org/10.1007/s40820-024-01495-1

 © Ariston Publications 2026. All rights reserved.

[30] Perdew, J.P., Burke, K. and Ernzerhof, M., **1996**. Generalized gradient approximation made simple. *Physical review letters*, *77*(18), p.3865. https://doi.org/10.1103/PhysRevLett.77.3865

[31] Papaspiropoulou, C., Michos, F.I., Aravantinos-Zafiris, N. and Sigalas, M.M., **2026**. Optical Absorption in Low-Dimensional AlxASx Nanostructures: Influence of Dimensional Extension and Exotic Geometries. *Solids*, *7*(4), p.34. https://doi.org/10.3390/solids7040034

[32] Ahlrichs, R., Bär, M., Häser, M., Horn, H. and Kölmel, C., **1989**. Electronic structure calculations on workstation computers: The program system turbomole. *Chemical Physics Letters*, *162*(3), pp.165-169. https://doi.org/10.1016/0009-2614(89)85118-8

[33] Furche, F., Ahlrichs, R., Hättig, C., Klopper, W., Sierka, M. and Weigend, F., **2014**. Turbomole. *Wiley Interdisciplinary Reviews: Computational Molecular Science*, *4*(2), pp.91-100. https://doi.org/10.1002/wcms.1162

[34] Frisch, M.J., Trucks, G.W., Schlegel, H.B., Scuseria, G.E., Robb, M.A., Cheeseman, J.R., Scalmani, G., Barone, V., Mennucci, B., Petersson, G.A. and Nakatsuji, H., **2009**. 09, Revision D. 01, Gaussian. *Inc., Wallingford, CT*, pp.20-44.

[35] Ernzerhof, M. and Scuseria, G.E., **1999**. Assessment of the Perdew–Burke–Ernzerhof exchange-correlation functional. *The Journal of chemical physics*, *110*(11), pp.5029-5036. https://doi.org/10.1063/1.478401

[36] Casida, M.E. and Huix-Rotllant, M., **2012**. Progress in time-dependent density-functional theory. *Annual review of physical chemistry*, *63*(1), pp.287-323. https://doi.org/10.1146/annurev-physchem-032511-143803

[37] Peach, M.J., Benfield, P., Helgaker, T. and Tozer, D.J., **2008**. Excitation energies in density functional theory: An evaluation and a diagnostic test. *The Journal of chemical physics*, *128*(4). https://doi.org/10.1063/1.2831900

© Ariston Publications 2026. All rights reserved.